3.
WATER-LOADED IMPROVED METAL DIAGONAL HORN TERMINATED IN BIO-MEDIUM/BIO-MEDIA

3.1 Introduction

The depth of penetration at microwave frequencies is generally shallow. Therefore, it is one of the research issues to design applicators to heat tumors lying at greater depth effectively. One category of real tumors may be classified as near spherical or oval-shaped. Although water-loaded conventional metal diagonal horn (MDH) provides circularly symmetric heating pattern, penetration depth (PD) in the biological media is not good enough. Therefore, it is thought to modify the aperture field distribution of the water-loaded conventional MDH without changing its aperture size in order to obtain enhanced PD in addition to symmetric effective field size (EFS) in the biological media. Considering these aspects, the author has modified the conventional MDH and named it the 'improved metal diagonal horn'. Improved metal diagonal horn (MDH) is a modified version of conventional MDH [Love (1976)] in which the aperture field is modified by introducing two pairs of conducting pins at appropriate locations near the horn aperture. In other words, the improved MDH is a changed version of conventional MDH. The concept of introducing conducting pins at appropriate positions inside the aperture has been suggested by Silver [Silver (1949)] for narrowing the H-plane beamwidth of an H-plane horn terminated in free space. Since the fields of an H-plane horn correspond to single TE_{10} mode, it has been suggested to use two pins inside the aperture in the reference [Silver (1949)] for reducing the H-plane beamwidth of the horn. However, conventional MDH is a multimode horn antenna in which the fields correspond to two orthogonal modes (TE_{10} and TE_{01}), which necessitates placing four conducting pins slightly inside the aperture of the horn for better focusing of the beam. Introduction of four conducting pins near the aperture generates aperture field corresponding to TE_{10}, TE_{30}, TE_{01}, and TE_{03} modes, which are significant (neglecting other higher order modes). Hence, field distribution over the aperture of improved MDH is a closer approximation to the uniform distribution that may ensure uniform absorbed-

power distribution in the bio-medium/bio-media and prevent steep power gradient in bio-media.

In this chapter, direct-contact water-loaded improved MDHs as hyperthermia applicators are investigated through simulation, theoretically and experimentally at 2450 MHz and through simulation and theoretically at 915 MHz. The proposed horns are assumed to be directly terminated in bio-medium/bio-media. Each improved MDH was filled with water to provide good impedance match between the horn and bio-medium/bio-media, which ensures good transmission into the bio-medium/bio-media.

3.2 Design and/or fabrication of water-loaded improved metal diagonal horns (MDHs)

Direct-contact water-loaded improved MDHs were designed at 2450 and 915 MHz and optimized using computer simulation technology microwave studio (CST MWS) 2011 software. Further, the horn designed at 2450 MHz was also fabricated to demonstrate the technical feasibility of the horn for hyperthermia. Geometry of water-loaded improved MDHs for operation at ISM frequencies of 2450 and 915 MHz is shown in Figure 3.1. The water-loaded conventional MDHs designed at 2450 and 915 MHz were transformed to corresponding water-loaded improved MDHs by introducing four metallic pins (whose ends touch the antenna walls) near each horn aperture at optimized locations parallel to antenna walls. The concept of introducing several metallic pins just inside the horn aperture for reducing H-plane beamwidth of an H-plane horn was first suggested by Silver [Silver (1949)]. Since H-plane horn fields correspond to single TE_{10} mode, two pins were used just inside the aperture in the example presented in reference [Silver (1949)]. However, conventional MDH antenna is a multimode horn antenna in which the fields correspond to two orthogonal modes (TE_{10} and TE_{01}). Therefore, two metallic pins each of radius 'r' (Table 3.1) are placed symmetrically on either side of centre at a distance of 'd_2' (Table 3.1) inside each horn aperture with inter-pin separation of 'd_3' (Table 3.1). Similarly, another pair of metallic pins in identical configuration is placed perpendicular to first pair of pins (Figure 3.1). The ends of the pins touch the horn walls. Neglecting the effect

of the modes of order higher than TE_{30} and TE_{03}, the resultant field over the aperture of each improved MDH corresponds to a combination of TE_{10}, TE_{30}, TE_{01}, and TE_{03} mode fields. At each antenna aperture, the fields of TE_{10} and TE_{01} modes combine out of phase with the fields of the modes TE_{30} and TE_{03} modes respectively. Hence, concentration of resultant field over the antenna aperture is shifted from central region (applicable for respective conventional MDHs) to the corner regions (applicable for the improved MDHs). This gives rise to more uniform field distribution over the aperture of each improved MDH that will ensure greater PD inside the biological phantom. Impedance matching is improved in the presence of pins when each improved MDH is in direct contact with the biological phantom.

Table 3.1: Design parameters of the water-loaded improved MDHs

Parameter	Symbol	Dimension (mm)	
		2450 MHz	915 MHz
Length of input waveguide	L_1	12	20
Transition length of circular waveguide	T_1	10	10
Length of circular waveguide	L_2	4	2
Diameter of circular waveguide	D	10	33.4
Transition length of square waveguide	T_2	10	12
Length of square waveguide	L_3	4	3
Throat size	d_1	9.4	29
Length of flaring section	L	46	106
Aperture size	d	24.6	65
Position of pin from the aperture	d_2	2.5	6.7
Separation between the pins	d_3	1.8	4.4
Radius of pins	r	1.5	4.2
Length of pins	d'	24	63

The apertures of each improved MDH antennas have been assumed to be surrounded by a conducting ground plane of copper in xy-plane so that the fringing electric field outside the aperture becomes zero. The dimensions of the conducting ground plane are 150 mm × 150 mm × 2 mm and 250 mm × 250 mm × 2 mm for the proposed improved MDHs designed at 2450 and 915 MHz respectively.

The dimension optimization of the proposed improved MDH antennas including the conducting pins was carried out through simulation. The optimized

dimensions of the improved MDH antennas are given in Table 3.1. Water-loaded improved MDH terminated in phantom bio-medium is shown in Figure 3.2(a). Figure 3.2(b) shows different views of the fabricated improved MDH antenna for operation at 2450 MHz.

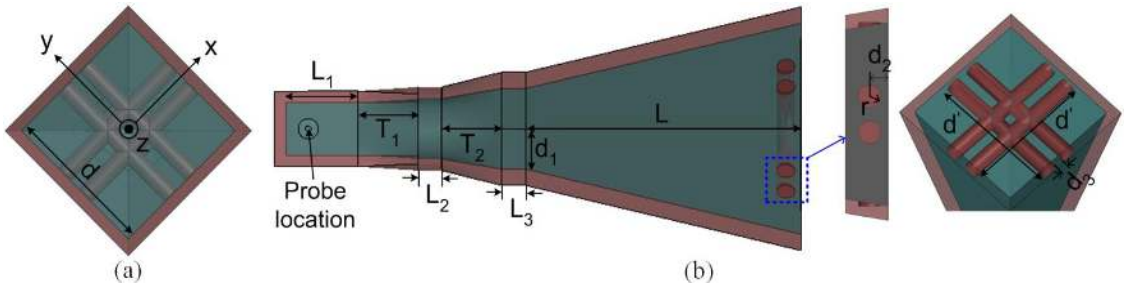

Figure 3.1: Geometry of water-loaded improved MDH antenna (a) top view, and (b) side view.

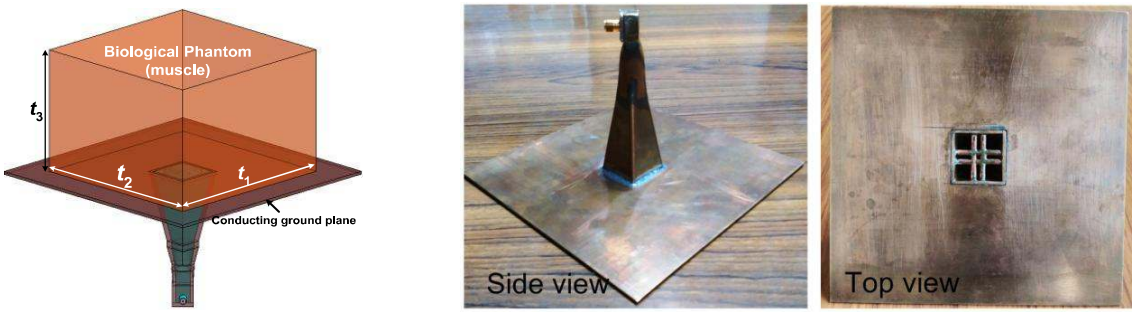

Figure 3.2: (a) Improved MDH antenna terminated in single layer bio-medium and (b) Different views of fabricated antenna for operation at 2450 MHz.

3.3 Water-loaded improved MDH terminated in phantom muscle

To study the modification of aperture field distributions of water-loaded improved MDHs designed at 2450 and 915 MHz due to introduction of conducting pins slightly inside the horn apertures, and the resulting SAR distributions in phantom muscle due to these horns simulation was performed. To verify the simulation results for aperture field distribution of the water-loaded improved MDHs designed at 2450 and 915 MHz theoretical analysis was carried out which includes the effect of higher order TE_{30} and TE_{03} modes also in addition to TE_{10} and TE_{01} modes. Higher order modes are excited due to the presence of conducting pins slightly inside the aperture of each horn. In addition, experimental study of SAR distribution in phantom muscle due to the horn designed at 2450 MHz was also carried out. The simulated results for SAR distribution in the

phantom bio-medium at 2450 MHz are compared with the corresponding theoretical and experimental results and the simulation results for SAR distribution at 915 MHz are compared with the corresponding theoretical results. The simulation of aperture field distributions of both the horn antennas and SAR distributions in phantom muscle due to these antennas was carried out using CST MWS software. The theoretical investigation of fields in the planar phantom muscle medium due to water-loaded improved MDH makes use of plane wave spectral technique for computation of SAR distribution in the medium. The theoretical field components, aperture field distributions and SAR distributions were numerically evaluated using MATLAB software. The experimental study of SAR distributions in the phantom bio-medium of known physical properties [Stuchly and Stuchly (1980)] at 2450 MHz was carried out with the help of 50 Ω coaxial L-shaped and straight monopole probes and Agilent make spectrum analyser (Model E4448A). The frequency of 2450 MHz was chosen for experimental study because of the availability of respective equipments components in the laboratory and also to verify the results with those obtained through simulation as well as theoretically.

3.3.1 *Analysis of electric field and specific absorption rate (SAR) in phantom muscle in direct contact with water-loaded improved MDH*

The proposed improved MDH antennas are improved versions of respective conventional MDHs in which the conventional diagonal horns are modified in order to enhance the PD in the biological phantom. In each improved MDH, two pairs of metallic pins are placed perpendicular to each other slightly inside the aperture of the conventional MDH as shown in Figure 3.1 (The details about the diameter of pins, their locations and the mode generated in each improved horn are already given in Section 3.2).

To study the modification of aperture field distributions of water-loaded improved MDHs in the presence of conducting pins due to the generation of higher order modes, theoretical analysis was carried out. Further, once aperture field distributions of antennas designed at 2450 and 915 MHz are known through theoretical analysis and evaluation using MATLAB software, theoretical

evaluation of induced electric fields in the phantom muscle and hence SAR distributions in the medium due to the horns, which are terminated in the bi-layered media consisting of muscle and free space layers, was done using plane wave spectral technique and MATLAB software. In the present analysis, the muscle layer is considered to be of finite thickness 't_3' followed by infinite free space layer. Muscle phantom and free space layers have relative permittivities of ε_1^* and ε_2 respectively. The complex relative permittivities of the biological phantom are equal to 50.00-j16.00 [Stuchly and Stuchly (1980)] and 55.00-j19.00 [Gabriel (1996)] at 2450 and 915 MHz respectively. The apertures of the improved MDHs are assumed to be surrounded by infinite conducting ground planes in xy-plane. The improved horns are multimode horns in which TE_{10}, TE_{30}, TE_{01} and TE_{03} modes exist at their apertures. In the present theoretical analysis, resultant aperture field distributions of the improved horns are obtained by combining the fields of two sets of orthogonal modes TE_{10}, TE_{30}, TE_{01}, and TE_{03} having specific excitation coefficients.

The x- and y-components of electric field at the apertures of improved MDHs [Silver (1949), Love (1976)] are represented by

$$E_{x_1}(x,y,0) = a_{10}(1+\Gamma_{10})\cos\left(\frac{\pi y}{d}\right)\exp(-j\beta_{10}d_2) + a_{30}(1+\Gamma_{30})\cos\left(\frac{3\pi y}{d}\right)\exp(-j\beta_{30}d_2) \tag{3.1}$$

$$E_{y_1}(x,y,0) = a_{01}(1+\Gamma_{01})\cos\left(\frac{\pi x}{d}\right)\exp(-j\beta_{01}d_2) + a_{03}(1+\Gamma_{03})\cos\left(\frac{3\pi x}{d}\right)\exp(-j\beta_{03}d_2) \tag{3.2}$$

where a_{10}, a_{01}, a_{30}, a_{03} are amplitude coefficients [Appendix-A], Γ_{10} , Γ_{01}, Γ_{30} Γ_{03} are reflection coefficients at the interface between the improved MDH of interest (designed at 2450/915 MHz) and muscle phantom for TE_{10}, TE_{01}, TE_{30} and TE_{03} modes respectively [Appendix-B]. The relations for corresponding phase constants β_{10}, β_{01}, β_{30}, and β_{03} are given by:

$$\beta_{10} = \beta_{01} = \frac{2\pi}{\lambda_\varepsilon}\left[1 - \left(\frac{\lambda_\varepsilon}{2\left(\frac{d+d'}{2}\right)}\right)^2\right]^{1/2} \tag{3.3}$$

$$\beta_{30} = \beta_{03} = \frac{2\pi}{\lambda_\varepsilon}\left[1 - \left(\frac{3\lambda_\varepsilon}{2\left(\frac{d+d'}{2}\right)}\right)^2\right]^{1/2} \tag{3.4}$$

where λ_ε (= $\lambda_0/\sqrt{\varepsilon_r}$) is effective wavelength, ε_r is the complex permittivity of water, λ_0 is free space operating wavelength, d is the aperture size of the improved MDH at the given design frequency, and $d' \times d'$ is the cross-sectional dimension of the corresponding horn opening at a depth d_2 from its aperture.

As the aperture of each proposed improved MDH is square, the phase constants for TE_{10} and TE_{01} modes are identical. Similarly, the values of phase constants for TE_{30} and TE_{03} modes are equal.

Once the field at the aperture of the improved horn designed at the given frequency is determined, field inside the biological phantom is derived by using plane wave spectral technique [Compton (1964), Harrington (1961)]. The x-, y-, and z-components of electric field in the biological phantom (layer1) are written as

$$E_{x1}(\mathrm{x,y,z}) = \frac{1}{2\pi^2}\int_{-\infty}^{\infty}\int_{-\infty}^{\infty}\left[-jk_{z1}I_{\psi_1}e^{-jk_{z1}z} + jk_{z1}R_{\psi_1}e^{jk_{z1}z}\right]e^{-jk_x x}e^{-jk_y y}dk_x dk_y \tag{3.5}$$

$$E_{y1}(\mathrm{x,y,z}) = \frac{1}{2\pi^2}\int_{-\infty}^{\infty}\int_{-\infty}^{\infty}\left[jk_{z1}I_{\phi_1}e^{-jk_{z1}z} - jk_{z1}R_{\phi_1}e^{jk_{z1}z}\right]e^{-jk_x x}e^{-jk_y y}dk_x dk_y \tag{3.6}$$

$$\begin{aligned} \mathrm{E}_{z1}(\mathrm{x,y,z}) = {} & \frac{1}{2\pi^2}\int_{-\infty}^{\infty}\int_{-\infty}^{\infty}\left[I_{\phi_1}e^{-jk_{z1}z} + R_{\phi_1}e^{jk_{z1}z}\right]e^{-jk_x x}(-\mathrm{j}k_y)e^{-jk_y y}dk_x dk_y \\ & -\frac{1}{2\pi^2}\int_{-\infty}^{\infty}\int_{-\infty}^{\infty}\left[I_{\psi_1}e^{-jk_{z1}z} + R_{\psi_1}e^{jk_{z1}z}\right](jk_x)e^{-jk_x x}e^{-jk_y y}dk_x dk_y \end{aligned} \tag{3.7}$$

where $I_{\psi_1}, I_{\phi_1}, R_{\psi_1}, R_{\phi_1}$ are plane wave spectra in muscle layer (layer 1), k_{z1} is the propagation constant in muscle layer along z-direction, and k_x and k_y are respectively the propagation constants along x- and y-directions.

And the x-, y- and z-components of electric field in free space layer (layer2) are written as

$$E_{x2}(\mathrm{x,y,z}) = \frac{1}{2\pi^2}\int_{-\infty}^{\infty}\int_{-\infty}^{\infty} -jk_{z2}T_{\psi_1}e^{-jk_{z2}z}e^{-jk_x x}e^{-jk_y y}dk_x dk_y \tag{3.8}$$

$$E_{y2}(\mathrm{x,y,z}) = \frac{1}{2\pi^2}\int_{-\infty}^{\infty}\int_{-\infty}^{\infty} jk_{z2}T_{\phi_1}e^{-jk_{z2}z}e^{-jk_x x}e^{-jk_y y}dk_x dk_y \tag{3.9}$$

$$\begin{aligned} E_{z2}(\mathrm{x,y,z}) = {} & \frac{1}{2\pi^2}\int_{-\infty}^{\infty}\int_{-\infty}^{\infty} T_{\phi_1}e^{-jk_{z2}z}e^{-jk_x x}(-\mathrm{jk}_y)e^{-jk_y y}dk_x dk_y \\ & -\frac{1}{2\pi^2}\int_{-\infty}^{\infty}\int_{-\infty}^{\infty} T_{\psi_1}e^{-jk_{z2}z}(-\mathrm{jk}_x)e^{-jk_x x}e^{-jk_y y}dk_x dk_y \end{aligned} \tag{3.10}$$

where T_{ψ_1} and T_{ϕ_1} are plane wave spectra in free space layer and k_{z2} is the propagation constant in free-space layer along z-direction.

Similarly, the x-, y- and z-components of magnetic field in the biological phantom and free space layers are derived.

By taking the inverse Fourier transform of equations (3.5) and (3.6) at z = 0, we get

$$jk_{z1}[-\mathrm{I}_{\psi_1} + \mathrm{R}_{\psi_1}] = f \tag{3.11}$$

where

$$f = \int_{-d/2}^{\mathrm{d}/2}\int_{-d/2}^{\mathrm{d}/2} \mathrm{a}_{10}(1+\Gamma_{10})\cos\left(\frac{\pi y}{d}\right)\exp(-\mathrm{j}\beta_{10}d_2) + \mathrm{a}_{30}(1+\Gamma_{30})\cos\left(\frac{3\pi y}{d}\right)\exp(-\mathrm{j}\beta_{30}d_2)e^{jk_x x}e^{jk_x y}dxdy$$

$$\text{or } f = \left(4\pi d\sin\left(\frac{k_x d}{2}\right)\cos\left(\frac{k_y d}{2}\right)\right)\left\{\frac{a_{10}(1+\Gamma_{10})\exp(-\mathrm{j}\beta_{10}d_2)}{k_x(\pi^2 - \mathrm{k}_y{}^2 d^2)} - \frac{a_{30}(1+\Gamma_{30})\exp(-\mathrm{j}\beta_{30}d_2)}{k_x(9\pi^2 - \mathrm{k}_y{}^2 d^2)}\right\}$$

$$\text{and } jk_{z1}[\mathrm{I}_{\phi 1} - \mathrm{R}_{\phi 1}] = g \tag{3.12}$$

where

$$g = \int_{-d/2}^{\mathrm{d}/2}\int_{-d/2}^{\mathrm{d}/2} \mathrm{a}_{10}(1+\Gamma_{01})\cos\left(\frac{\pi x}{d}\right)\exp(-\mathrm{j}\beta_{01}\mathrm{d}_2) + \mathrm{a}_{03}(1+\Gamma_{03})\cos\left(\frac{3\pi x}{d}\right)\exp(-\mathrm{j}\beta_{o3}\mathrm{d}_2)e^{jk_x x}e^{jk_x y}dxdy$$

$$\text{or } g = \left(4\pi d\sin\left(\frac{k_y d}{2}\right)\cos\left(\frac{k_x d}{2}\right)\right)\left\{\frac{a_{01}(1+\Gamma_{01})\exp(-\mathrm{j}\beta_{01}\mathrm{d}_2)}{k_y(\pi^2 - \mathrm{k}_x{}^2 d^2)} - \frac{a_{03}(1+\Gamma_{03})\exp(-\mathrm{j}\beta_{o3}\mathrm{d}_2)}{k_y(9\pi^2 - \mathrm{k}_x{}^2 d^2)}\right\}$$

By applying the boundary conditions, *i.e.* the continuity of tangential electric and magnetic fields at 'z = t_3' (the interface between muscle and free-space), remaining four equations are determined as follows:

$$-jk_{z1}I_{\psi_1}e^{-jk_{z1}t_3} + jk_{z1}R_{\psi_1}e^{jk_{z1}t_3} = -jk_{z2}T_{\psi_1}e^{-jk_{z2}t_3} \tag{3.13}$$

$$jk_{z1}I_{\phi_1}e^{-jk_{z1}t_3} - jk_{z1}R_{\phi_1}e^{jk_{z1}t_3} = jk_{z2}T_{\phi_1}e^{-jk_{z2}t_3} \tag{3.14}$$

$$\begin{aligned}&\left(k_1{}^2 - k_x{}^2\right)\left[I_{\phi_1}e^{-jk_{z1}t_3} + R_{\phi_1}e^{jk_{z1}t_3}\right] - k_xk_y\left[I_{\psi_1}e^{-jk_{z1}t_3} + R_{\psi_1}e^{jk_{z1}t_3}\right]\\ &= \left(k_2{}^2 - k_x{}^2\right)T_{\phi_1}e^{-jk_{z2}t_3} - k_xk_yT_{\psi_1}e^{-jk_{z2}t_3}\end{aligned} \tag{3.15}$$

$$\begin{aligned}&\left(k_1{}^2 - k_y{}^2\right)\left[I_{\psi_1}e^{-jk_{z1}t_3} + R_{\psi_1}e^{jk_{z1}t_3}\right] - k_xk_y\left[I_{\phi_1}e^{-jk_{z1}t_3} + R_{\phi_1}e^{jk_{z1}t_3}\right]\\ &= \left(k_2{}^2 - k_y{}^2\right)T_{\psi_1}e^{-jk_{z2}t_3} - k_xk_yT_{\phi_1}e^{-jk_{z2}t_3}\end{aligned} \tag{3.16}$$

The expressions for R_{ψ_1} and R_{ϕ_1} obtained from equations (3.11) and (3.12) are substituted into equations (3.13) – (3.16) and by solving the resulting equations, plane wave spectra I_{ψ_1}, I_{ϕ_1}, R_{ψ_1}, R_{ϕ_1}, T_{ψ_1} and T_{ϕ_1} were determined and hence the expression for electric field induced in the biological phantom is derived.

The x-, y-, and z-components of electric field in the biological phantom can then be found by using equations (3.5–3.7). The resultant electric field intensity in the synthetic muscle is given by

$$|E|^2 = |E_{x1}|^2 + |E_{y1}|^2 + |E_{z1}|^2 \tag{3.17}$$

The SAR in the phantom muscle can be evaluated by

$$SAR = \frac{\sigma|E|^2}{2\rho} \tag{3.18}$$

where ρ and σ are respectively the density and conductivity of the biological phantom.

3.3.2 *Results and discussion*

3.3.2.1 *Applicators' characteristics*

The applicators' design data and dielectric property of phantom muscle medium given in sections 3.2 and 3.3, and Table 3.3 have been used to obtain the

simulated values of input reflection coefficient of the improved MDH antennas in direct contact with phantom muscle medium at the operating frequencies of 2450 and 915 MHz. The simulated values of input reflection coefficient of the antennas terminated in the phantom muscle medium are -31 dB and -20 dB respectively at 2450 and 915 MHz, while the measured value of input reflection coefficient for the horn designed at 2450 is -15 dB.

Moreover, reflection coefficient at the interface of each improved MDH applicator and the biological phantom has also been estimated theoretically as mentioned in sub-section 3.3.1 and Appendix-B. The estimated value of the said reflection coefficient for TE_{10} and TE_{01} modes of the improved horn designed at 2450 MHz is -25 dB and that for TE_{30} and TE_{03} modes is -35 dB. Similarly, corresponding reflection coefficients values for the horns designed at 915 MHz are -27.8 dB and -32.4 dB respectively.

3.3.2.2 *Aperture electric field distributions and SAR distributions in phantom muscle*

3.3.2.2.1 *Simulated aperture electric field distribution*

The effective heating of the biological phantom depends strongly on the size of the antenna aperture and the field distribution across it. The electric field distributions over the apertures of the improved MDHs designed at 2450 and 915 MHz were determined through simulation. Figures 3.3 and 3.4 depict the simulated electric field distributions over the aperture of the horns designed at 2450 and 915 MHz. It can be seen from Figure 3.3(a) and 3.4(a) that in the absence of pins (conventional MDH), the amplitude of electric field intensity at the apertures of these horns goes down near their periphery due to propagation of TE_{10} and TE_{01} modes.

The effect of two pairs of pins on the aperture field distribution of each improved MDH was studied through simulation. In the beginning, two pins were placed parallel to the aperture of the horn designed at 2450 MHz along x-direction as shown in Figure 3.3(b). The electric field distribution becomes symmetrical about x-axis and the maximum of electric field intensity shifts from central region to the side regions of the horn cross section when two pins are placed on either

side of centre parallel to x-axis. A dip in the electric field intensity is also obtained on each side of x-axis along y-direction due to the presence of pins. In the next phase another pair of pins was placed on either side of centre parallel to y-axis. In this case, the description about electric field distribution similar to that provided for the case of pins parallel to x-axis applies with x-axis/y-direction interchanged. The combination of four pins placed slightly inside the aperture provides the simulated aperture field distribution shown in Figure 3.3(c) for the horn designed at 2450 MHz. The enhancement of aperture field near the corners of the improved MDH designed at 2450 MHz can be observed from Figure 3.3(c). Therefore, the simulated electric field distribution across the aperture of improved MDH has become more uniform as compared with the conventional MDH at the design frequency of 2450 MHz. Similar arguments apply for the improved MDH designed at 915 MHz for which the aperture field distributions in absence and in presence of two pairs of conducting pins are shown in Figures 3.4(a) and 3.4(b).

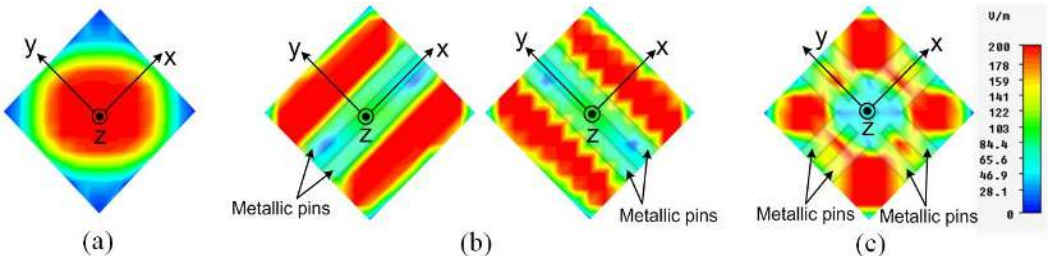

Figure 3.3: Simulated field distribution(s) at the aperture of (a) conventional MDH, (b) horn with pins along x-and y-directions, and (c) improved MDH, all designed at 2450 MHz.

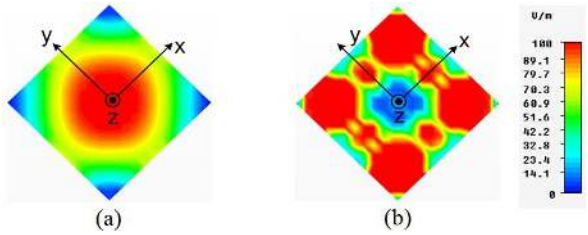

Figure 3.4: Simulated field distribution at the aperture of (a) conventional MDH, and (b) improved MDH, both designed at 915 MHz.

3.3.2.2.2 *Theoretical aperture electric field distribution*

The theoretical aperture electric field distribution of the improved MDHs designed at 2450 and 915 MHz were obtained by evaluating the field expressions (Equations 3.1 and 3.2) using MATLAB software by assuming power orthogonality and the results are presented in Figures 3.5, 3.6 and 3.7.

Since the theoretical results for aperture field distribution depend on the amplitude excitation coefficients for higher order modes also in addition to fundamental modes, the effect of amplitude excitation coefficients of higher order modes (generated due to presence of conducting pins) on aperture field distributions of the improved MDHs designed at 2450 and 915 MHz was studied theoretically (Figures 3.5 and 3.6). The values of excitation coefficients of different modes to get more uniform field distribution at the aperture of the improved MDH of interest are optimized keeping in view the following factors: (i) The aperture field distribution of the horn of interest in presence of two pairs of conducting pins is modelled in terms of distribution corresponding to TE_{10} and TE_{01} modes along with TE_{30} and TE_{03} modes (generated due to presence of conducting pins) assuming that excitation coefficient of TE_{10} mode, a_{10} equals the excitation coefficient of TE_{01} mode and sum of powers (= Input power/2) carried by TE_{10} and TE_{30} modes is equal to sum of powers (= Input power/2) carried by TE_{01} and TE_{03} modes, (ii) the aperture field distribution of the horn in presence of pins along x-direction is given in terms of distribution corresponding to TE_{10}, TE_{30} (generated due to presence of conducting pins) and TE_{01} modes with respective excitation coefficients of a_{10}, a_{30}, and a_{01} (= a_{10}), whose value with respect to a_{10} is to be optimized . The electric fields due to TE_{10} and TE_{30} modes combine out of phase at the horn aperture while the field corresponding to TE_{01} mode is orthogonal to those associated with TE_{10} and TE_{30} modes, (iii) Similarly, the aperture field distribution of the horn in presence of pins along y-direction can be viewed to have been produced due to TE_{10}, TE_{01} and TE_{03} modes with respective excitation coefficients of a_{10}, a_{01} and a_{03} (= a_{30}), whose value with respect to a_{01} is to be optimized. Again, the electric fields corresponding to TE_{01} and TE_{03} modes combine out of phase at the horn aperture while the field corresponding to TE_{10} mode is orthogonal to those for TE_{01} and TE_{03} modes. From Figures 3.5 and 3.6, it can be seen that optimized excitation coefficients of TE_{10}, TE_{01}, TE_{30}, and TE_{03} modes for the horns with two pairs of conducting pins designed at 2450 and 915 MHz are found to be $1/d\sqrt{1.81}$, $1/d\sqrt{1.81}$, $0.9/d\sqrt{1.81}$, and $0.9/d\sqrt{1.81}$ respectively. The aperture field distributions of the horns designed at 2450 and

915 MHz for optimized excitation coefficients of different modes are shown in Figures 3.5(c) and 3.6(c) respectively.

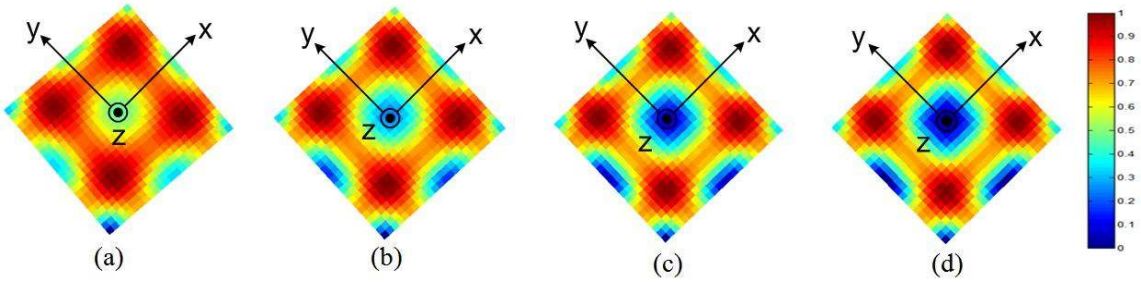

Figure 3.5: Predicted normalized field distribution at the aperture of improved MDH at 2450 MHz for different values of excitation coefficients $a_{30}/a_{10} = a_{03}/a_{01}$, (assuming $a_{30} = a_{03}$ and $a_{10} = a_{01}$) (a) 0.5, (b) 0.7, (c) 0.9, and (d) 1.

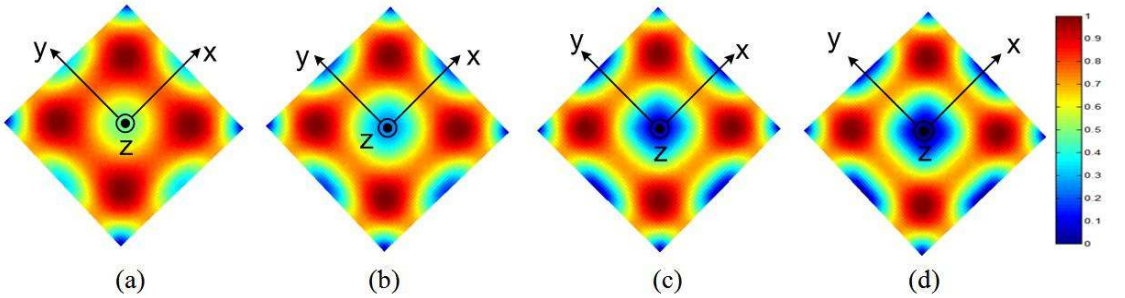

Figure 3.6: Predicted normalized field distribution at the aperture of improved MDH at 915 MHz for different values of excitation coefficients $a_{30}/a_{10} = a_{03}/a_{01}$, (assuming $a_{30} = a_{03}$ and $a_{10} = a_{01}$) (a) 0.5, (b) 0.7, (c) 0.9, and (d) 1.

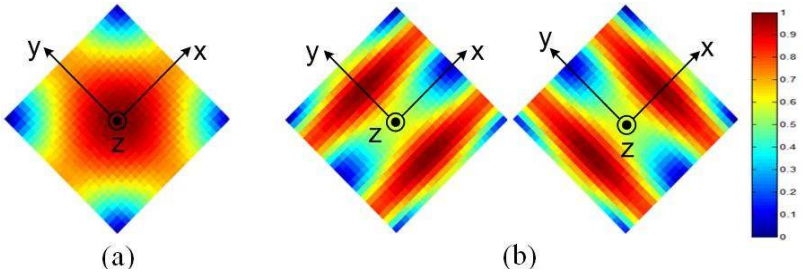

Figure 3.7: Predicted normalized field distribution(s) at the aperture of (a) conventional MDH, and (b) horn with pins along x- and y-directions.

A representative example of predicted aperture field distributions of the horn designed at 2450 MHz without and with pins along x- and y-directions for corresponding optimized excitation coefficients are shown in Figure 3.7. Note that for the horn without conducting pins (conventional MDH), only TE_{10} and TE_{01} modes exist at the horn aperture with equal power carried by each mode [Figure 3.7(a)]. The aperture field distribution of conventional MDH under study is modified by placement of conducting pins oriented along x- and y-directions at a distance 'd_2' inside the horn aperture. Nearly identical simulated and predicted

field distributions at the horn aperture in presence of conducting pins along x-/y-direction [Figures 3.3(b) and 3.7(b)] verifies the assumption that higher order TE_{30} and TE_{03} modes having optimized excitation coefficients combine in aforementioned phases with the fields of TE_{10} and TE_{01} modes having identical excitation coefficients to produce the resulting aperture illumination of the horn.

Similar arguments can be applied for the proposed improved MDH designed at 915 MHz for which the predicted aperture field distributions in presence of two pairs of conducting pins for optimized excitation coefficients of different modes are shown in Figure 3.6(c).

It can be observed from Figures 3.3–3.7 that simulated aperture illumination of the improved MDHs are nearly in agreement with the corresponding theoretical illumination.

3.3.2.2.3 *Simulated SAR distributions in phantom muscle medium*

The density and conductivity of the phantom muscle medium used in simulation study of SAR distributions are given in Table 3.3. The simulated relative SAR distributions inside the phantom bio-medium (muscle) of size $t_1 \times t_2 \times t_3$ = 112 mm × 112 mm × 80 mm and 200 mm × 200 mm × 150 mm due to the improved MDHs designed at 2450 and 915 MHz respectively are determined and the results are shown in Figures 3.8 and 3.9. Initially, the power fed to each antenna was assumed to be 1W in the simulation study. The relative SAR distributions in the biological phantom are obtained by normalizing the SAR values with respect to the maximum value of SAR that occurs in the biological phantom at the given frequency.

Effect of size and position of metallic pins on simulated SAR distributions

Metallic pins placed near the apertures of the improved MDHs play an important role in modifying the aperture field distributions and hence the SAR distribution in the biological phantom. In order to evaluate the effect of pin dimensions on SAR distribution, parametric study has been performed through simulation at 2450 and 915 MHz.

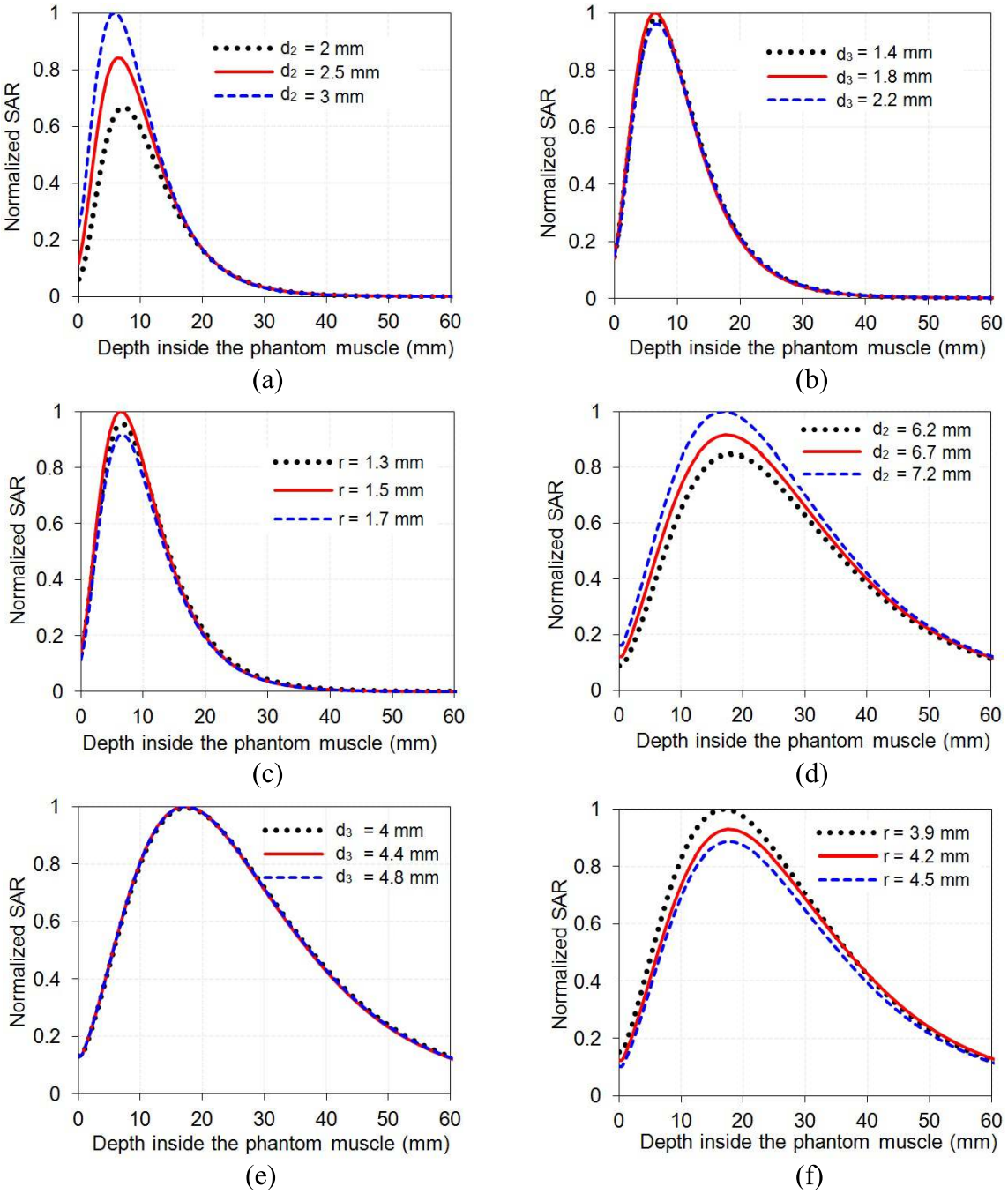

Figure 3.8: Effects of (a) pins' location 'd_2' at 2450 MHz, (b) inter-pin spacing 'd_3' at 2450 MHz, (c) pins' radius 'r' at 2450 MHz, (d) pins' location 'd_2' at 915 MHz, (e) inter-pin spacing 'd_3' at 915 MHz, (f) pins' radius 'r' at 915 MHz on normalized SAR distributions along z-direction in phantom muscle due to the improved MDH antennas for 1 W input power.

Figure 3.8(a) shows the effect of pins' position (d_2) inside the aperture of the improved MDH antenna designed at 2450 MHz on the relative SAR distribution in the phantom muscle. It is clear from Figure 3.8(a) that PD in the phantom muscle medium decreases with increase in the value of d_2. The optimum value of d_2 (= 2.5 mm) provides maximum PD and appropriate peak SAR value in the

phantom muscle due to the improved horn designed at 2450 MHz. Figure 3.8(b) illustrates the effect of separation between metallic pins (d_3) placed at optimum distance inside the aperture of the improved MDH antenna (designed at 2450 MHz) on the relative SAR distribution in the biological phantom. It can be observed from Figure 3.8(b) that as we change the separation between the metallic pins from optimum value of 1.8 mm, slight reduction in the values of PD and peak SAR occurs. Figure 3.8(c) depicts the effect of radius '*r*' of metallic pins on the relative SAR distribution in the phantom muscle at 2450 MHz. It is observed from Figure 3.8(c) that as we change the radius of metallic pins from the optimum value of 1.5 mm, reduction in the values of PD and peak SAR occurs again. It is to be noted that the values of peak absolute SAR used for normalization of SAR distribution curves given in Figure 3.8(a), (b), (c) for the improved MDH designed at 2450 MHz are respectively equal to 47.9, 36.9, 36.9 W/kg respectively.

Similar arguments apply for the improved MDH designed at 915 MHz and the variations of relative SAR distributions in the phantom muscle medium due to the proposed antenna at 915 MHz for different values of d_2, d_3 and r including the corresponding optimized values are given in Figure 3.8(d), 3.8(e), 3.8(f). Additionally, the values of peak absolute SAR used for normalization of SAR distribution curves given in Figure 3.8(d), (e), (f) for the improved MDH designed at 915 MHz are respectively equal to 2.31, 2.11, 2.28 W/kg respectively.

3.3.2.2.4 *Theoretical SAR distributions in phantom muscle medium*

Theoretical normalized SAR distributions in the biological phantom at 2450 and 915 MHz due to the improved MDHs were obtained by numerically solving the equations given in section 3.3 (derived by using plane wave spectral technique) using MATLAB software and the results are given in Figure 3.9.

3.3.2.2.5 *Experimental SAR distribution in phantom muscle medium at 2450 MHz*

The experimental study of relative SAR distributions in the phantom bio-medium of known physical properties [Stuchly and Stuchly (1980)] at 2450 MHz was carried out with the help of 50 Ω coaxial L-shaped and straight monopole

probes and Agilent make spectrum analyser (Model E4448A). The relative SAR distributions in the phantom muscle medium of size 112 mm × 112 mm × 80 mm due to the horn designed at 2450 MHz were measured following the procedure given in chapter 2 and the experimental results are given in Figures 3.9(a) and 3.9(b).

3.3.2.2.6 *Comparison of simulated, theoretical and/or experimental SAR distributions*

Figure 3.9(a) and 3.9(c) illustrates the relative SAR distributions in the homogeneous phantom muscle in z-direction for the improved MDHs designed at 2450 and 915 MHz. Different curves of the relative SAR distributions were obtained by normalizing the absolute SAR values of the curves with respective peak absolute SAR values (reference values). That is why, value of maximum normalized SAR value for all described curves is identical. The values of simulated, theoretical and/or experimental PD in biological phantom (depth where relative SAR value is down to 13.5 percent of the maximum in the tissue) extracted from Figure 3.9(a) and 3.9(c) are given in Table 3.2 for the improved diagonal horns.

The EFS is defined as the area that is enclosed within 50% SAR contour in the transverse plane of the phantom bio-medium. The simulated, theoretical and experimental values of EFS in the homogeneous bio-medium extracted from Figures 3.9(b) and 3.9(d) due to the improved MDH designed at the given frequency 2450/915MHz are nearly in agreement with each other and exhibit circular symmetry (Table 3.2). Each improved MDH has almost identical aperture illumination in E- and H-planes. That is why, it provides circularly symmetric SAR distribution in the transverse plane. Further, it can be observed from Table 3.2 that the simulated values of PD and EFS in the biological phantom are close to the respective theoretical and/or experimental values. The deviation in the results for PD and EFS may be due to (i) the generation of other higher order modes not taken into account in the theoretical analysis, and (ii) fabrication and measurement errors.

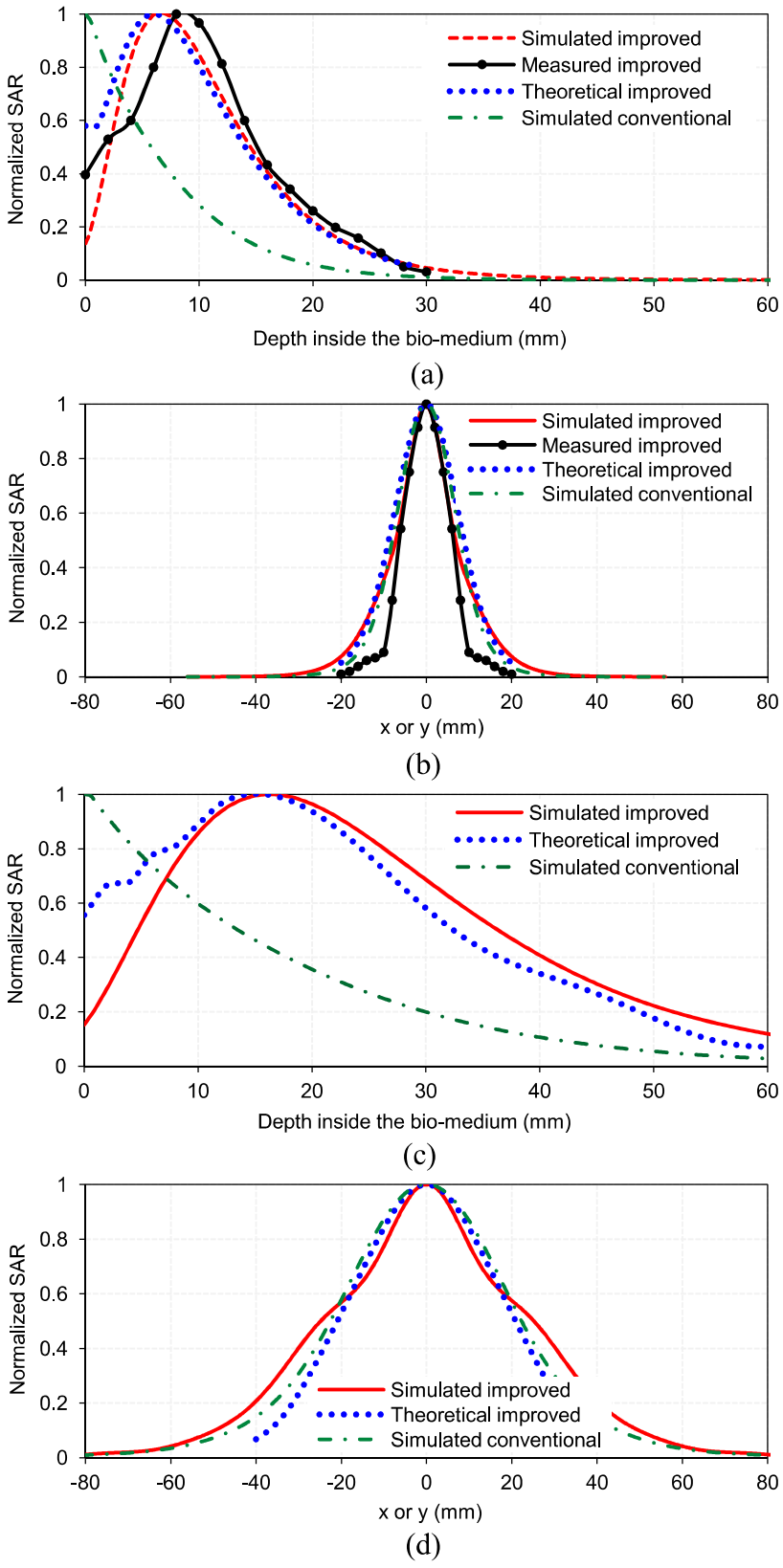

Figure 3.9: Normalized SAR distributions inside the phantom muscle due to improved/conventional MDHs along (a) z-direction (x = y = 0) at 2450 MHz, (b) x-/y-direction at z = 10 mm (y/x = 0) at 2450 MHz, (c) z-direction (x = y = 0) at 915 MHz, and (d) x-/y-direction at z = 20 mm (y/x = 0) at 915 MHz.

Further, the simulated normalized SAR distributions along z- and x-/y-directions due to the improved MDHs are compared with those due to the corresponding conventional MDHs (Figure 3.9). It can be seen from Figure 3.9 and Table 3.2 that the improved MDHs provide greater PD though almost same EFS in the biological phantom as compared with their conventional counterparts. This is made possible due to the presence of metallic pins near the aperture of the improved diagonal horn at the given frequency (2450/915 MHz) which produces more uniform field distribution at its aperture as compared with the corresponding conventional antenna.

Table 3.2: SAR parameters in the muscle medium owing to the improved/conventional MDHs

SAR parameters			Frequency (MHz)	
			2450	915
PD (mm)	Simulated	Improved MDH	23.4	58.5
		Conventional MDH	15	36
	Theoretical Improved MDH		23	54
	Measured Improved MDH		25	–
EFS (mm^2)	Simulated	Improved MDH	14 × 14	50 × 50
		Conventional MDH	16 × 16	44 × 44
	Theoretical Improved MDH		17 × 17	45 × 45
	Measured Improved MDH		13 × 13	–

3.4 Simulation study on water-loaded improved MDHs terminated in tri-layered bio-media without and with tumor

The work presented in preceding sections is extended by performing simulation study on two water-loaded improved MDHs (designed at 2450 and 915 MHz), each in direct contact with tri-layered bio-media (skin, fat and muscle layers) without and with embedded tumor for determination of SAR and temperature distributions using CST MWS software.

Three tri-layered bio-models were taken for study through simulation at each frequency (Figure 3.10). First bio-model pertains to tri-layered bio-media (skin, fat and muscle layers) without tumor. Second bio-model consists of tri-layered bio-media with oval-shaped abdominal /limb tumor lying inside the muscle tissue while the third involves tri-layered bio-media with irregular-shaped

abdominal/limb tumor lying inside muscle the muscle tissue. The locations of oval- and irregular-shaped tumors lying within second and third tri-layered bio-models considered for each of the applicators designed at 2450 and 915 MHz are provided in Figure 3.11. In all, four tumors of different shapes/sizes (two for each of the applicators) were considered in the present study. For heating of tumors designated as tumor1 (oval-shaped) and tumor2 (irregular-shaped), water-loaded improved MDH antenna designed at 2450 MHz which is in direct contact with tri-layered bio-media containing these tumors (one at a time) was considered. For heating of tumors designated as tumor3 (oval-shaped) and tumor4 (irregular-shaped), water-loaded improved MDH antenna designed at 915 MHz which in direct contact with tri-layered bio-media containing the aforesaid tumors (one at a time) was considered. A cancerous tissue is known to have higher water content [Michaelson and Lin (1987)] and therefore higher dielectric constant and conductivity. The detailed dimensions and dielectric/physical properties of different layers of bio-media and tumors are given in Figure 3.11/Table 3.3. It is to be noted that size of tumor3 and tumor4 considered in this chapter is larger as compared with tumor3/tumor4 considered in chapter 2 because of larger heating volume in the media due to improved MDH.

3.4.1 *SAR distributions without and with tumor*

The normalized SAR distributions in the bio-media without tumor due to the improved MDHs designed at 2450 and 915 MHz are depicted in Figures 3.12–3.15. The values of PD and EFS extracted from Figures 3.12-3.15 are given in Table 3.4. It can be seen that the values of PD and EFS are significantly higher at 915 MHz as compared to those at 2450 MHz.

To observe the effect of tumor embedded in the muscle layer simulations were performed for the improved MDHs (designed at 2450 and 915 MHz), each terminated in tri-layered bio-media with embedded tumor and the corresponding normalized SAR distributions are depicted in Figures 3.12-3.15.

Figures 3.12 and 3.13 show the simulated variations of normalized SAR distributions in the inhomogeneous tri-layered bio-media without/with embedded

tumor, along z-direction (for x = y = 0) at 2450 and 915 MHz respectively due to the water-loaded improved MDHs whereas Figures 3.14 and 3.15 show the variations of normalized SAR distributions in the aforesaid configurations of bio-media along x-/y-directions at 2450 and 915 MHz respectively due to the respective improved horns. The values of PD and EFS for the frequencies of 2450 MHz and 915 MHz extracted from Figures 3.12-3.15 are given in Table 3.4. It can be seen from Table 3.4 that the values of PD and EFS in the bio-media are significantly higher at 915 MHz as compared to those at 2450 MHz. Further, the presence of a tumor does not alter PD and EFS (in the centre of tumor) significantly in each case. Additionally, it is observed that values of PD in the tri-layered bio-model due to the water-loaded improved MDH designed at 2450 and 915 MHz are sufficient to cover whole tumor depth for effective hyperthermia. Also, relative SAR value observed at the skin surface using each of the water-loaded improved MDH applicators is minimum.

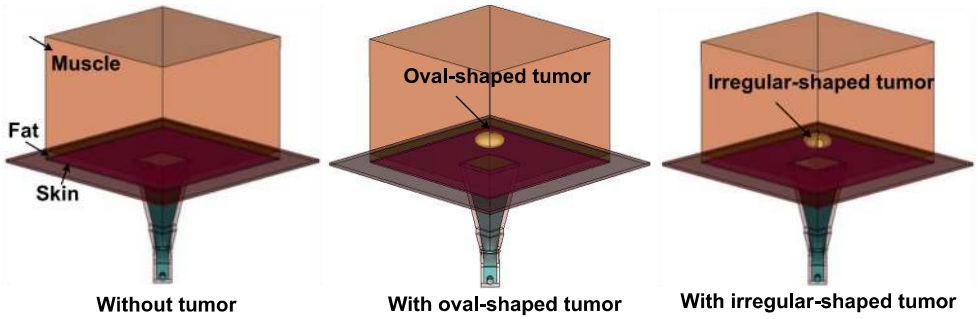

Figure 3.10: Improved MDH antenna designed at a given frequency and terminated in tri-layered bio-media.

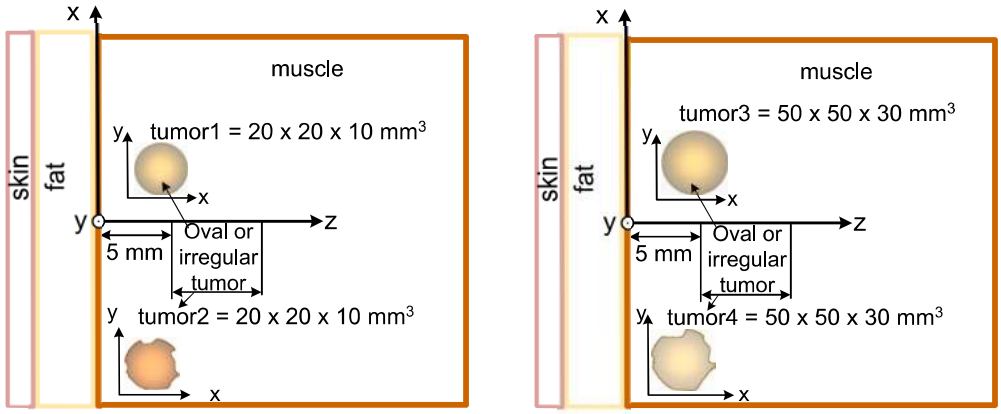

Figure 3.11: Two-dimensional realistic tri-layered bio-model with embedded (a) tumor1/tumor2 (applicable for the improved MDH designed at 2450 MHz) and (b) tumor3/tumor4 (applicable for the improved MDH designed at 915 MHz).

Table 3.3: Properties of bio-media and tumor [Stuchly and Stuchly (1980), Gabriel (1996)].

Tissue/Tumor	Thickness (mm)	Density (kg/m^3)	ε_r at 2450 MHz	ε_r at 915 MHz
Skin	1	1130	42-j12	46-j16.7
Fat	5	920	5.28-j0.76	11.3-j2.16
Muscle	80	1050	50-j16	55-j19
Tumor1/Tumor2	10	1050	56-j21.3	-
Tumor3/Tumor4	30	1050	-	58-j21.6

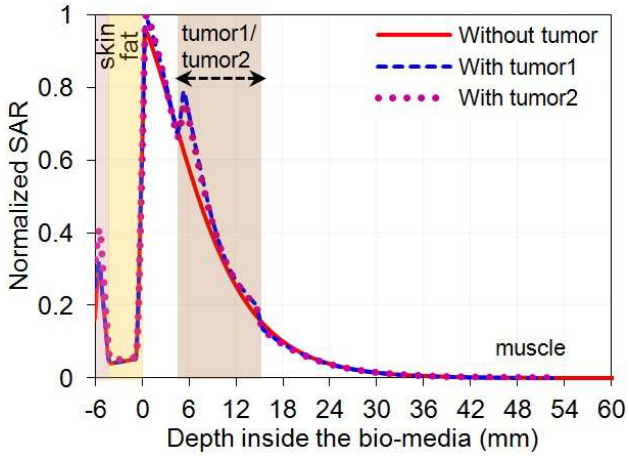

Figure 3.12: Simulated normalized SAR distributions inside the bio-model without and with embedded tumor1/tumor2 due to improved MDHs at 2450 MHz along z-direction (x = y = 0).

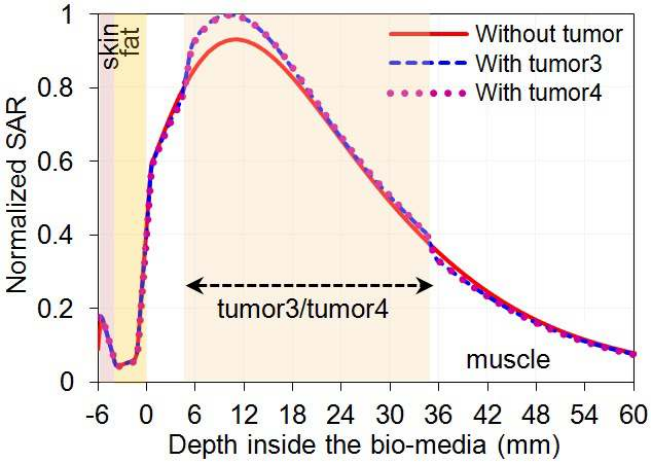

Figure 3.13: Simulated normalized SAR distributions inside the bio-model without and with embedded tumor3/tumor4 due to improved MDHs at 915 MHz along z-direction (x = y = 0).

3.4.2 *Temperature distributions without and with tumor*

In order to characterize the hyperthermia treatment system, inhomogeneous tri-layered bio-models fed through water-loaded improved MDHs were considered as shown in Figure 3.10. The thermal simulation was performed by CST multi-

physics simulator software at an initial temperature of 37°C. The thermal parameters of the bio-media used in simulation are same as given in chapter 2.

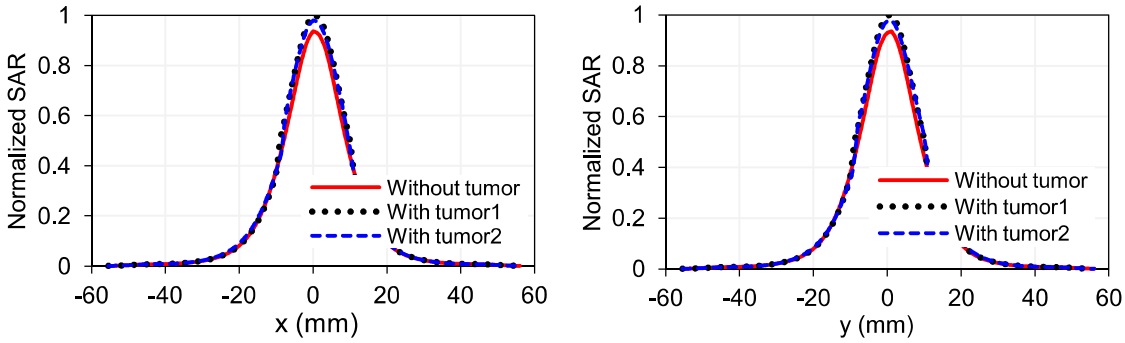

Figure 3.14: Simulated normalized SAR distributions inside the bio-models due to the improved MDH at 2450 MHz along (a) x-direction at z = 10 mm (middle of tumor1/tumor2) (y = 0), and (b) y-direction at z = 10 mm (middle of tumor1/tumor2) (x = 0).

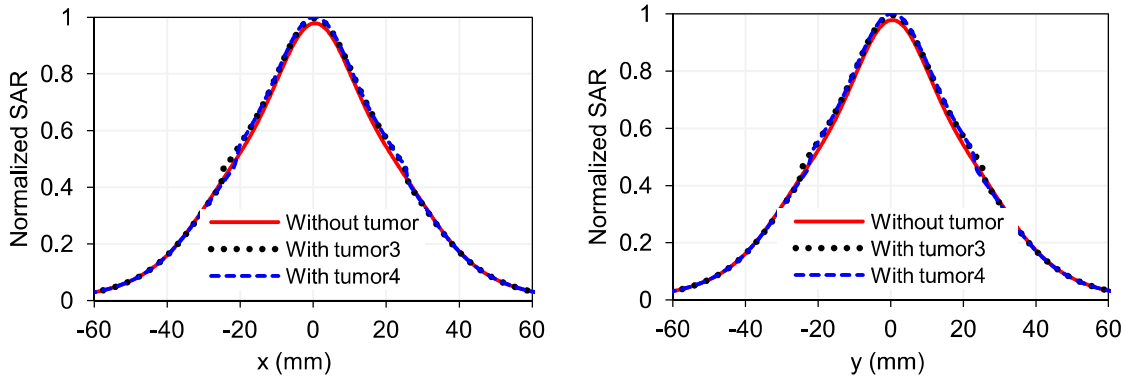

Figure 3.15: Simulated normalized SAR distributions inside the bio-models due to the improved MDH at 915 MHz along (a) x-direction at z = 20 mm (middle of tumor3/tumor4) (y = 0), and (b) y-direction at z = 20 mm (middle of tumor3/tumor4) (x = 0).

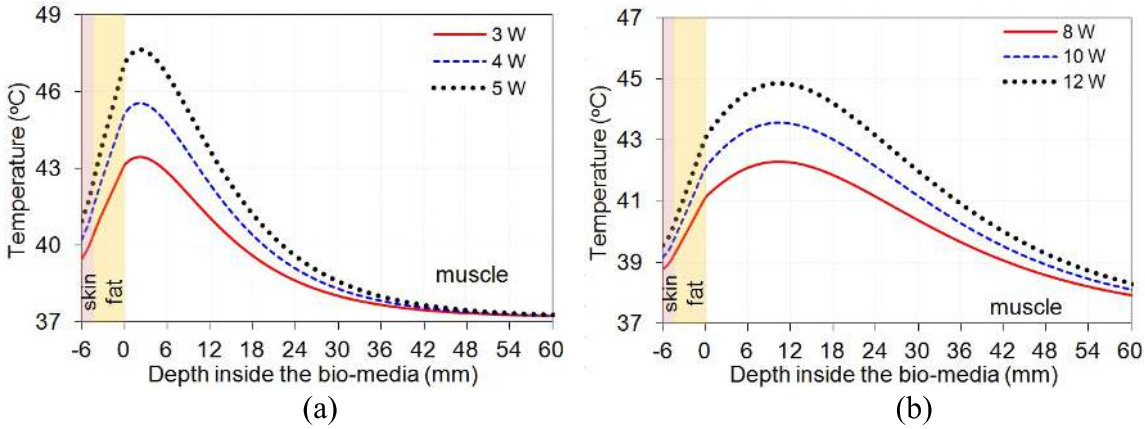

Figure 3.16: Temperature distribution inside the tri-layered bio-media without tumor for different input power levels along z-direction (x=y=0) due to improved MDH at (a) 2450 MHz and (b) 915 MHz.

Figure 3.16(a) and (b) shows the variations of temperature as a function of depth in the tri-layered bio-model without tumor due to water-loaded improved MDHs designed at 2450 and 915 MHz respectively by taking input power level as a parameter. It can be seen from Figure 3.16 that as the power fed to the applicator increases, the temperature in the bio-media rises. As expected the temperature decreases exponentially with depth inside the bio-media. It can be inferred from Figure 3.16 that the desired temperature range (41–45 ^{o}C) for effective hyperthermia was achieved for input power level of 4 and 10 W for the improved antennas designed at 2450 and 915 MHz respectively.

Figure 3.17(a) and (b) show the variations of temperature in the biological media with time due to the water-loaded improved MDHs designed at 2450 and 915 MHz respectively for corresponding normal bio-model without tumor and the bio-model with embedded irregular tumor (tumor2 considered at 2450 MHz and tumor4 at 915 MHz) by taking tumor depth as a parameter. It is noticed that tumor temperature in each case reaches to a higher value as compared with normal tissue temperature [Figure 3.17(a) and (b) and Table 3.4]. This would aid in effective preferential heating of tumor in the superficial region of the body in comparison to normal tissue. Further, it can be observed from Figure 3.17(a) and (b) that initial rate of rise of temperature is higher at lower depth in the realistic tri-layered bio-media for optimum input power of 4 and 10 W respectively at the frequencies of 2450 and 915 MHz. The rate of rise of temperature in each case slows down after 20 minutes of heating and the tissue temperature approaches a steady value after about 50 minutes of heating at a given depth. The results demonstrate that tissue temperature approaches saturation after certain time period of heating at a given depth and shows decreasing trend as the depth in the muscle medium increases.

Figure 3.18(a) and (b) show the profiles of temperature along z-direction in the inhomogeneous tri-layered bio-media without and with embedded tumor at the frequencies of 2450 and 915 MHz respectively due to the respective water-loaded improved MDHs by taking tumor configuration as a parameter.

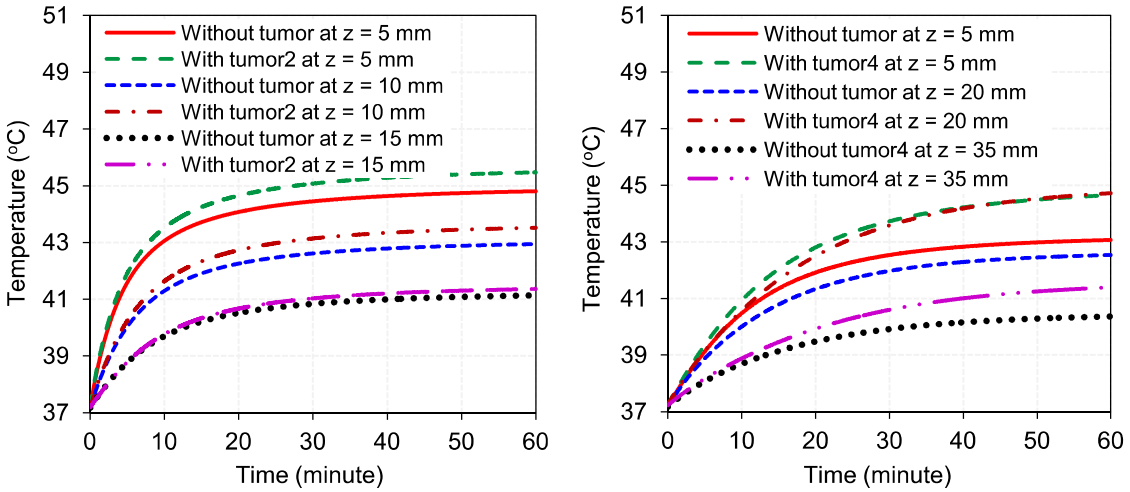

Figure 3.17: Variations of temperature with time due to the improved MDHs in the realistic tri-layered bio-media without and with embedded (a) tumor2 for x = y = 0 at 2450 MHz, (b) tumor4 for x = y = 0 at 915 MHz.

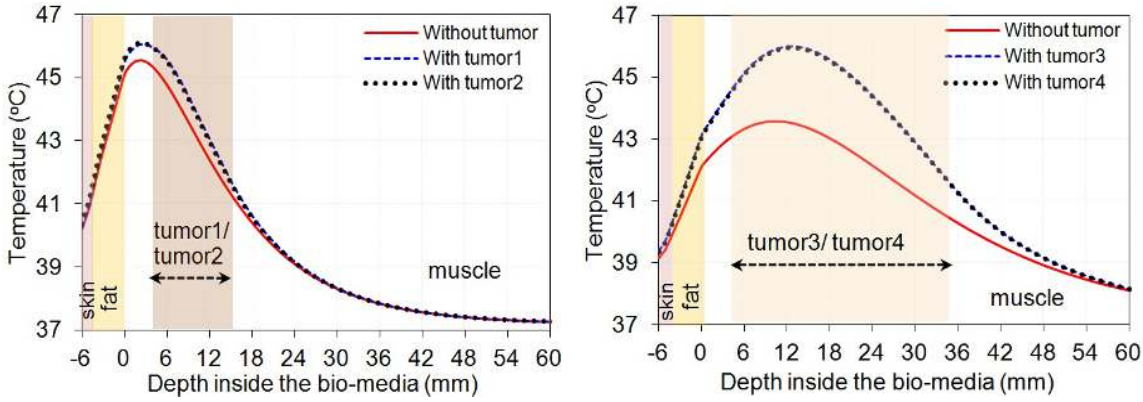

Figure 3.18: Simulated temperature distributions inside the tri-layered bio-models without and with embedded tumors along z-direction (x = y = 0) due to the improved horn at (a) 2450, and (b) 915 MHz.

It can be observed from Figure 3.18 that temperature profiles are similar for different tumor shapes. Moreover, applicator designed at 915 MHz provides enhanced values of PD in bio-models as compared to those at 2450 MHz (Figure 3.18 and Table 3.4). The values of peak temperature elevation (PTE) and the depth at which temperature elevation reduces to half of the maximum in the realistic tri-layered bio-models (obtained through thermal simulation) are also given in Table 3.4. It is observed from Table 3.4 that presence of tumor increases PTE in the tissue at each frequency. Further, the depth at which temperature elevation is half of the maximum with respect to initial temperature (=ΔT/2) [derived from Figure 3.18(a) and (b) in each case] is given in Table 3.4. It can be

noted from Table 3.4 that the depth at ΔT/2 is higher at 915 MHz as compared to that at 2450 MHz though presence or absence of tumor has insignificant effect on this depth. Further, it is observed that the presence of tumor of one configuration or another affects to certain degree the temperature distribution along the depth at both the frequencies of interest. Moreover, heating temperature at skin-fat interface is less than 41 ^{o}C at both ISM frequencies (Figure 3.18).

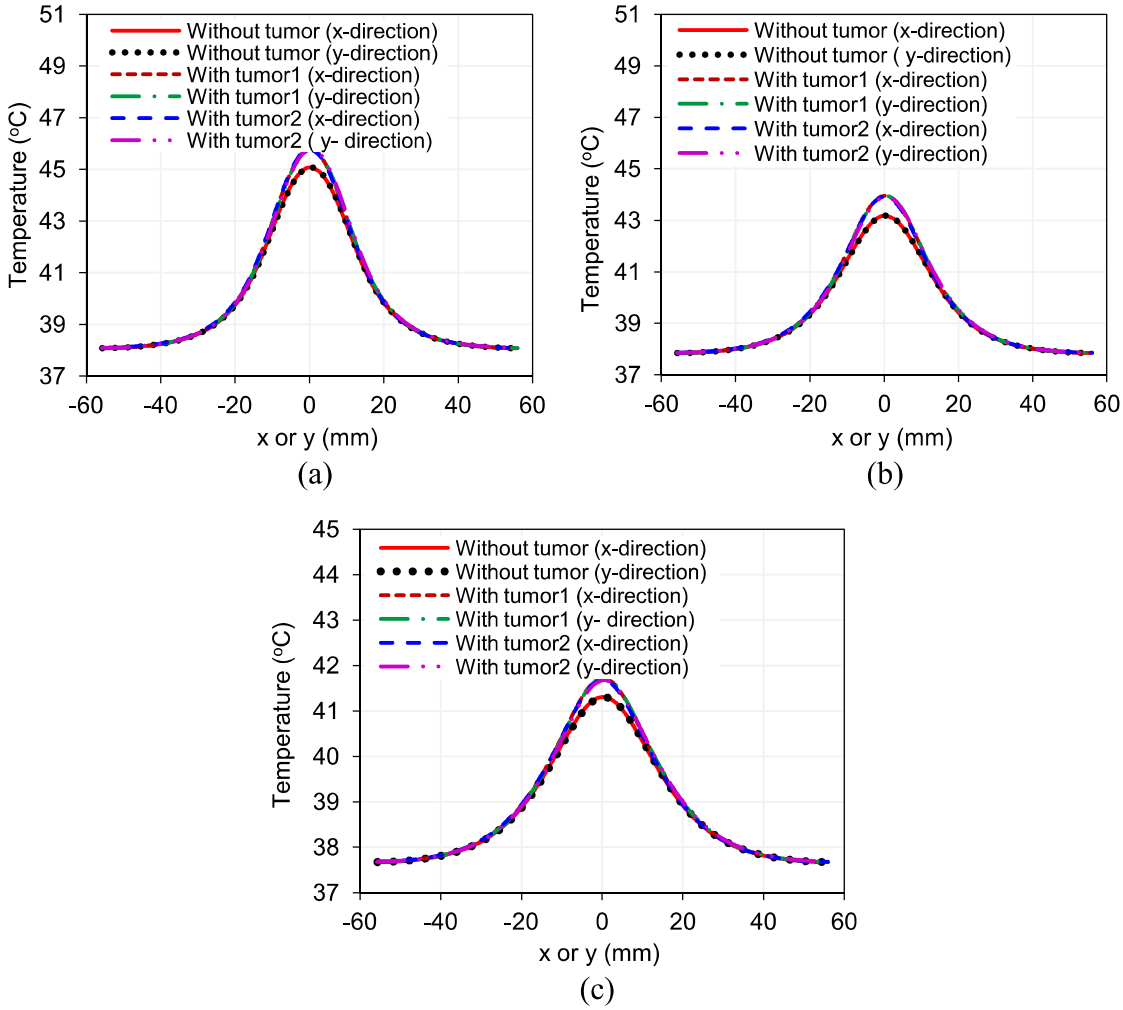

Figure 3.19: Simulated temperature distributions inside the tri-layered bio-model without tumor, with embedded tumor1 and with embedded tumor2 along x-/y-direction (y/x=0) at (b) z = 5 mm, (b) z = 10 mm, and (c) z= 15 mm, due to the improved MDH at 2450 MHz for optimum input power of 4 W.

Figure 3.19(a), (b) and (c) illustrates the profiles of temperature distribution in the three bio-models: bio-models without tumor, with embedded tumor1 and embedded tumor2 along x-/y-direction (y/x=0) due to the water-loaded improved MDH designed at 2450 MHz for optimum input power of 4 W for different depths

in the tumor z = 5, 10 and 15 mm respectively. Figure 3.20(a), (b) and (c) depicts the profiles of temperature distribution in another set of three bio-models: bio-models without tumor, with embedded tumor3 and embedded tumor4 along x-/y-direction (y/x=0) due to the water-loaded improved MDH designed at 915 MHz for optimum input power of 10 W for different depths in the tumor z = 5, 20 and 35 mm respectively. The results depict that tumors of different shapes/sizes are effectively heated owing to the associated improved horns.

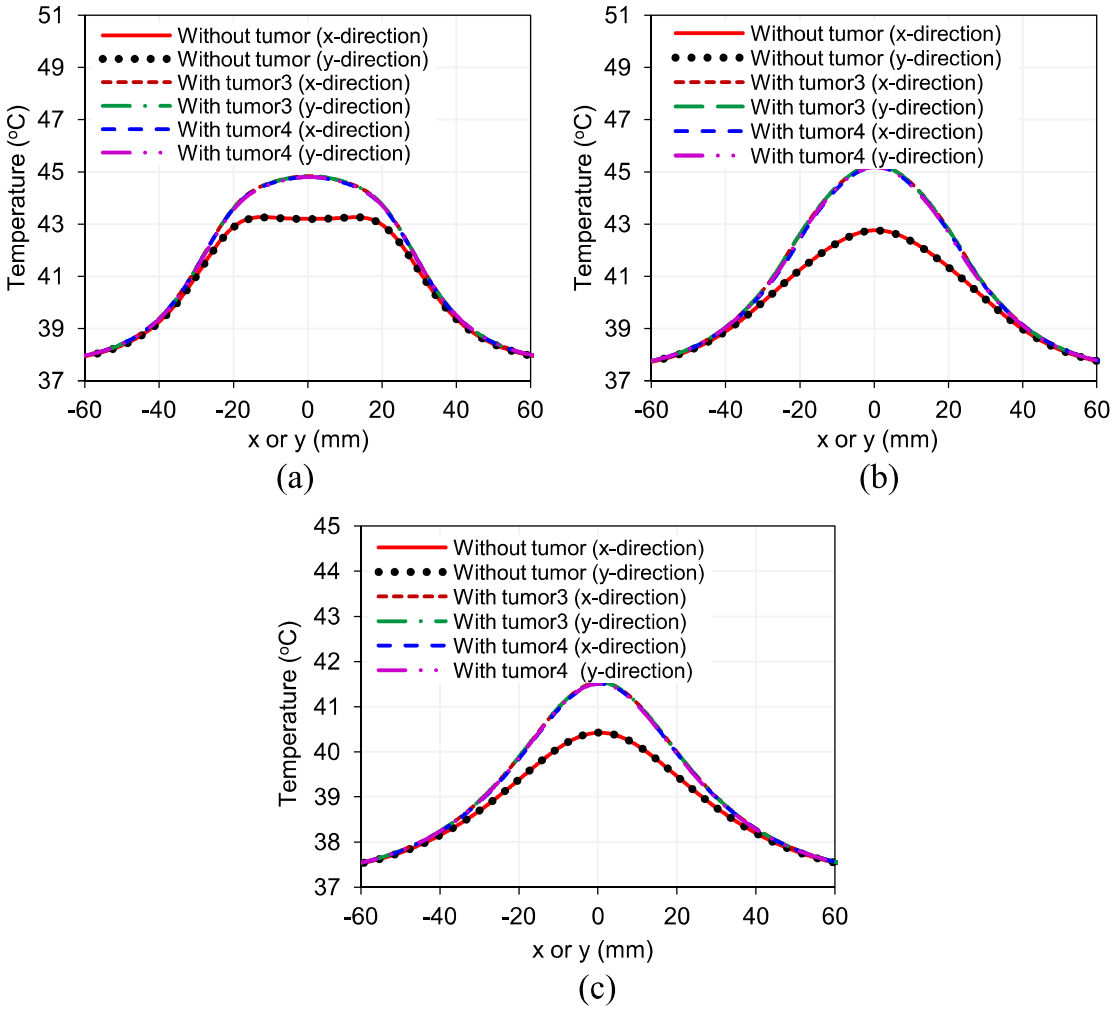

Figure 3.20: Simulated temperature distributions inside the tri-layered bio-model without tumor, with embedded tumor3 and with embedded tumor4 along x-/y-direction (y/x=0) at (b) z = 5 mm, (b) z = 20 mm, and (c) z= 35 mm, due to the improved MDH designed at 915 MHz for 10 W input power.

Figure 3.21(a), (b), (c) and (d) shows the cross-sectional profiles of temperature distribution in the bio-media without and with tumor1/tumor2 in xz plane (for y=0), yz plane (for x=0), with embedded tumor1 in xy plane for z = 6, 10, and 14 mm; and with embedded tumor2 in xy- plane for z = 6, 10, and 14 mm

respectively owing to the water-loaded improved MDH designed at 2450 MHz. Figure 3.22(a), (b), (c) and (d) shows the cross-sectional profiles of temperature distribution in the bio-models without and with tumor3/tumor4 in xz plane (for y =0), yz plane (for x =0), with embedded tumor3 in xy plane for z = 6, 20, and 34 mm; and with embedded tumor4 in xy- plane for z = 6, 20, and 34 mm respectively owing to the water-loaded improved MDH designed at 915 MHz.

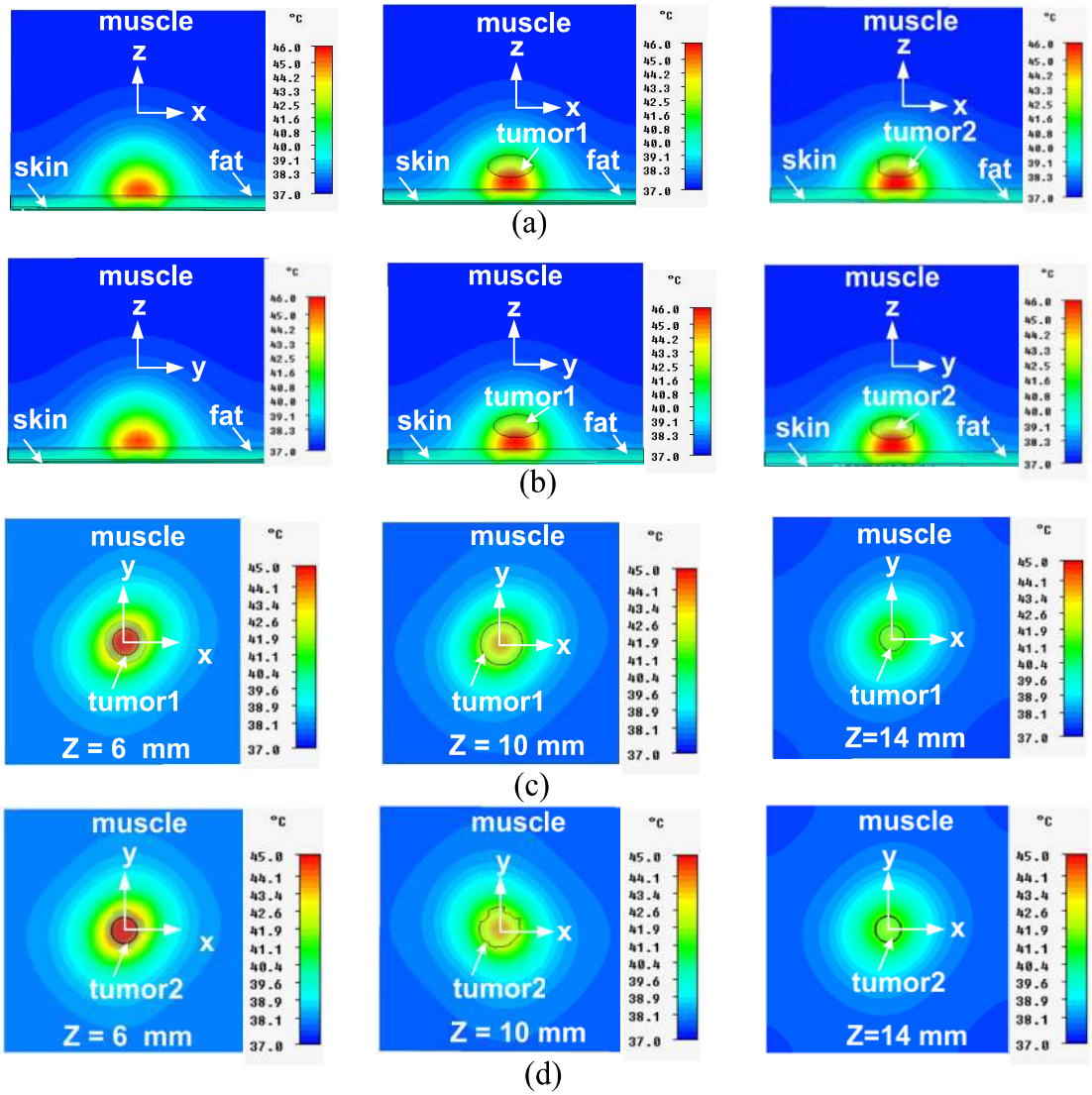

Figure 3.21: Temperature distributions inside the realistic tri-layered bio-media without and with embedded tumor1/tumor2 due to the improved MDH at 2450 for 4 W input power in (a) xz-plane, (b) yz-plane, (c) xy-plane with tumor1, and (d) xy-plane with tumor2.

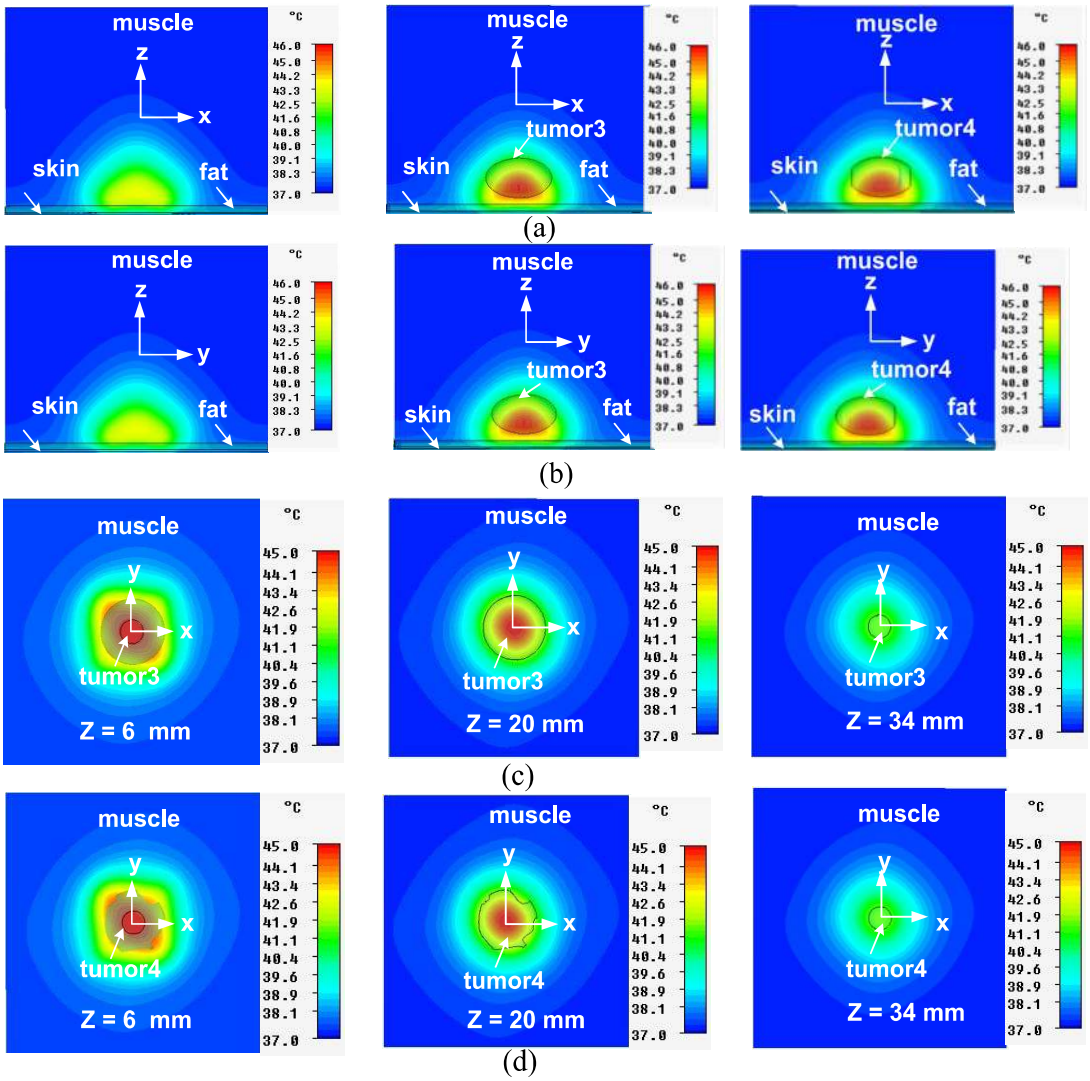

Figure 3.22: Temperature distributions inside the realistic tri-layered bio-media without and with embedded tumor3/tumor4 due to the improved MDH at 915 MHz for 10 W input power in (a) xz-plane, (b) yz-plane, (c) xy-plane with tumor3, and (d) xy-plane with tumor4.

It can be observed that antenna designed at 915 MHz provides wider heating area and enhanced heating depth in bio-model as compared to those at 2450 MHz. It is again apparent from Figures 3.21 and 3.22 that the tumors are effectively heated using the associated improved MDH applicators. It can be seen that desired temperature range (41 – 45 ^{o}C) is maintained in the respective tumor for effective hyperthermia in each case. Further, symmetrical temperature distributions in the bio-media due to the improved applicators can be observed in the transverse xy-plane [Figures 3.21(c), (d) and 3.22(c), (d)].

Table 3.4: Hyperthermia performance due to the water-loaded MDH applicators

Freq. (MHz)	Inhomogeneous model	PD (mm)	EFS[$] ($mm^2$)	PTE (^oC)	Depth at ΔT/2 (mm)	Heating area[$] {41-45$^oC$} ($mm^2$)
2450	Without tumor	22.5	18 × 18	8.55	21.1	24.1× 24.1
	With tumor1	21.6	18.84 × 18.84	9.05	21.5	25.6 × 25.6
	With tumor2	21.4	18 ×18.8	9.10	21.3	25.5 × 25.6
915	Without tumor	58.5	44.3 × 44.3	6.58	42	44.8 × 44.8
	With tumor3	56.8	46.6 × 46.6	8.99	41.2	55.2 × 55.2
	With tumor4	56.9	45 × 45.5	8.94	41.5	53.8 × 54.2

[$]EFS and heating area are defined in the middle of tumor.

3.5 Chapter summary

In the present chapter, water-loaded improved MDHs have been investigated through simulation, theoretically and/or experimentally for hyperthermia application at 2450 and 915 MHz. The study involved determination of SAR and temperature distributions in a planar biological phantom/realistic tri-layered bio-media without and with embedded tumors due to the water-loaded improved MDHs. Results obtained through simulation, theoretical and/or experimental studies indicate that the improved MDHs give higher PD in the homogeneous biological phantom/tri-layered bio-model as compared with the respective conventional diagonal horns. Further, the proposed improved MDH designed at 915 MHz and terminated in tri-layered bio-media provides higher PD and EFS as compared to those at 2450 MHz. The diagonal horns reported in the present chapter provide simple and effective means to enhance the PD in the biological model. The temperature distributions in the realistic bio-models obtained through thermal simulation indicate that the improved horns with 4 and 10 W input power at 2450 and 915 MHz respectively can be used as effective hyperthermia applicators for oval-/irregular-shaped tumors in superficial abdominal/thoracic region of the body.

In the next chapter, the investigation of water-loaded metal-dielectric-wall diagonal horn is presented for hyperthermia application.